CrossMark

RESEARCH PAPER

Soft chemistry synthesis route toward Bi$_2$Te$_3$ hierarchical hollow spheres

J. Fouineau · J. Peron · S. Nowak · M. Giraud · M. Sicard · S. Ammar-Merah · L. Sicard

Abstract Hollow spheres made of Bi$_2$Te$_3$ nanoplatelets were successfully synthesized using a low temperature, wet chemical synthesis route. By using a one-pot synthesis, large quantities of microspheres, arranged in a gypsum flower manner, can be obtained in about 1 h. The mechanism leading to such a particular morphology has been deeply studied by both solid and solution characterization techniques (X-ray diffraction, scanning and transmission electron microscopy, X-ray fluorescence, ^{1}H nuclear magnetic resonance spectroscopy) which were carried out at different stages of the synthesis. The key points are the generation of alcanethiol-in-polyol droplets and the subsequent in situ controlled interfacial reaction between Te and Bi precursors. The Te(IV) ions present in the alcanethiol phase are initially reduced

into Te(0) by decanethiol. The Bi(III) ions initially dissolved in the polyol phase are then reduced at the decanethiol/polyol interface, resulting in the progressive growth of Bi$_2$Te$_3$ hexagonal nanoplatelets at the outer surface of the pristine Te(0) sphere.

Introduction

Hollow micro/nanostructured spheres are now playing an important role in optics, optoelectronics, therapeutics, catalysis, etc. as well as in energy conversion technologies such as solar cells, fuel cells, and lithium batteries (Lai et al. 2012). These materials present inherent advantages since they provide enhanced surface-to-volume ratio and reduce transport lengths for both mass and charge transports. Three distinct strategies can be commonly used to produce a hierarchical hollow structure: hard templating in which a "rigid" template is used [e.g. silica (Wang et al. 2006), polymer latex spheres (Lu et al. 2004), and metal nanoparticles (Gao et al. 2006; Sun et al. 2003)], soft templating making use of relative flexible structures such as liquid droplets (Li et al. 2003; Yang and Zeng 2004), micelles or gas bubbles (Guo et al. 2007; Zhu et al. 2009), and template-free methods in which the material self-assembles into the desired structure.

J. Fouineau · J. Peron (✉) · S. Nowak ·
M. Giraud · S. Ammar-Merah · L. Sicard (✉)
Univ Paris Diderot, Sorbonne Paris Cité, ITODYS, UMR 7086 CNRS, 15 rue J-A de Baïf, 75205 Paris Cedex 13, France
e-mail: jennifer.peron@univ-paris-diderot.fr

L. Sicard
e-mail: lorette.sicard@univ-paris-diderot.fr

M. Sicard
ONERA, The French Aerospace Lab, BP 80100, 91123 Paris, Palaiseau, France

These preparative methods are more successful for metal oxides than for noble metals (Hu et al. 2011). For the synthesis of metallic hollow or cage-bell nanomaterials, only a few specific methods can be applied to a small number of metals (mostly Au, Ag, and Pt) and are based on other principles such as galvanic replacement, Kirkendall effect, Ostwald ripening, and layer-by-layer assembly (Liu et al. 2012).

In soft templating methods, the reactants are dissolved in two different and non-miscible phases. They, thus, react at the interface. For inorganic materials preparation, this method has been exploited both in conventional (Nakashima and Kimizuka 2003) and microfluidic systems (Zhao and Middelberg 2013) for oxide preparation in which the continuous phase contains the metal precursors and the droplets contain water molecules which will progressively hydrolyze the precursor at the water/solvent interface and lead to the formation of metal oxide hollow spheres. Nevertheless, no binary metallic systems have been prepared in such manner, and a general approach to rationally produce hollow structures for a wide spectrum of metals or alloys is still lacking today.

Herein, we describe a novel route allowing the preparation of nanostructured hollow spheres of Bi_2Te_3 by interfacial synthesis in a biphasic polyol-thiol droplet solution. Polyols are well known for their ability to dissolve organometallic complex or metal salt precursors due to their high dielectric constant as well as for their reducing power under relatively mild conditions. Moreover, the polyol process permits the synthesis of shape- and size-controlled nanoparticles (Brayner et al. 2013; Fievet 2000; Fievet et al. 1989). The nanoparticles obtained can be dispersed in polar solvents, which facilitate biological and environmental applications. We focused our attention on Bi_2Te_3 since, as an important semiconductor material with a high Seebeck coefficient and a high power factor, it has attracted much attention regarding thermoelectric applications. It was shown that its properties are greatly enhanced when the particle size is reduced down to the nanoscale (Kanatzidis 2010). The formation of hollow Bi_2Te_3 microstructures can potentially be beneficial for thermoelectric properties. Indeed, the small particle size causes scattering of the heat carrying phonons along the crystal boundaries, allowing to reduce efficiently the thermal conductivity while maintaining the electrical conductivity. In

addition, the void volumetric fraction of hollow Bi_2Te_3 microstructures could potentially reduce thermal conductivity while ensuring electrical percolation by the interconnected nanoparticles of the shell. Moreover, void fraction can be potentially filled with other components which will further decrease thermal conductivity while maintaining high electrical conductivity in the resulting hybrid material. In contrast to the top-down strategy, bottom-up assembly uses nanoparticles as building blocks to fabricate three-dimensional hetero-structured materials. This strategy is potentially more easily scalable and low cost. Bi_2Te_3 or Bi_2Te_3 alloys with different morphologies, including nanoparticles (Kim et al. 2010b, 2011), nanorods (Kim et al. 2010a; Purkayastha et al. 2006), nanowires (Mott et al. 2011), nanoplates or nanoplatelets (Mehta et al. 2010; Son et al. 2012; Soni et al. 2012), and nanospheres (Jiang et al. 2007) have been synthesized from a bottom-up strategy. Microsphere bouquets of Bi_2Te_3 nanoplates were also obtained, but this particular morphology was induced by nanoplate aggregation upon aging (Wang et al. 2010).

The present work reports a new strategy in which, using a facile one-pot synthesis, large quantity of nanostructured Bi_2Te_3 hollow microspheres can be obtained in about 1 h. The successful synthesis of Bi_2Te_3 spherical aggregates of nanoplatelets by a soft chemistry route is realized using a mixture of immiscible solvents, a polyol and an alcanethiol. This approach is based on the differential solubility of two inorganic salts and exploits both the ability of thiols to form complexes and the high dielectric constant of polyol to dissolve the inorganic precursors. The reducing abilities of both alcanethiol and polyol allow us to obtain nanostructured micro-Bi_2Te_3 hollow spheres. This study provides a comprehensive understanding of hollow sphere formation mechanisms and empirical guidelines for the high-yield synthesis of nanostructured Bi_2Te_3 micro-hollow spheres.

Materials and methods

Microsphere synthesis

$BiCl_3$ (99.9 %) and $TeCl_4$ (99.9 %) were purchased from Alfa-Aesar; other reagents were purchased from Aldrich and were used without further purification. In a typical synthesis, 0.5 mmol of bismuth chloride and

0.75 mmol of tellurium chloride were added in a three-necked flask containing 30 ml of ethylene glycol (EG). The inorganic precursors were dissolved into the EG for about half an hour under Ar flow. Then, 12.3 mmol of 1-decanethiol (DT) was added at once using a syringe. At this point, the mixture was allowed to stir for 10 more minutes at room temperature under Ar flow. The solution was then heated up to 180 °C with a ramp of 6 °C min^{-1} and refluxed under Argon flow for typically 1 h. The solution was then cooled down to room temperature; the particles were washed five times with dried acetone and centrifuged at 22,000 rpm with 10 min for each run. The resulting black powder was dried under vacuum at room temperature and stored in a desiccator.

^{1}H NMR of decanethiol: δH_a: 2.51 ppm, dd; δH_b: 1.60 ppm, quint.; δH_c: 1.37 ppm, m; δH_k: 1.31 ppm, t; δH_{d-i}: 1.26 ppm, m; δH_j: 0.88 ppm, t, and didecyldisulfide: $\delta H_{a'}$: 2.67 ppm, t; $\delta H_{b'}$: 1.66 ppm, quint.; $\delta H_{c'}$: 1.37 ppm, m; $\delta H_{d'-i'}$: 1.26 ppm, m; $\delta H_{j'}$: 0.88 ppm, t.

Characterization techniques

^{1}H NMR and HSQC-NMR spectra were recorded in CDCl$_3$ or C$_3$D$_6$O as the solvent with a 400 MHz Bruker AVANCE III spectrometer. GC/MS investigations were carried out with a VARIAN 450GC/320MS. The column used is a factor four fused silica capillary column (phase type: VF5 ms, length: 60 m, internal diameter: 0.25 mm, phase thickness: 1 μm). The carrier gas is helium. X-ray diffraction (XRD) patterns were recorded with a capillary spinner by using a PANALYTICAL EMPYREAN diffractometer with Cu Kα radiation ($\lambda = 1.5419$ Å), a focusing X-ray mirror, a multichannel PIXcel detector and in the 2θ range 10°–90° with a step size of 0.0263° (during 120 s). Rietveld's software MAUD 2.33 was used to fit the X-ray patterns and determine the respective abundances of the different phases. The analysis of the powder chemical composition was obtained with a PANalytical Epsilon 3xl X-ray fluorescence (XRF) spectrometer. The Ag anode X-ray tube was operated at a tube voltage of 50 kV and a tube current of 300 μA. The powder was deposited onto a polycarbonate film under air (time to proceed: 20 s). A silver cover and a spinner were used for the experiments, and the calibration was performed on standard solutions of Bi and Te from Aldrich. The measured peaks for standards and samples are Lα for Bi and Kα for Te. The morphology of the samples was observed, and their thickness was determined with a field emission scanning electron microscope (SEM-FEG) model Zeiss supra 40. Transmission electron microscopy (TEM) images and high resolution TEM images were performed on a JEOL JEM 100CX with a camera CCD Soft Imaging System (Keenview Pro) and an accelerating voltage of 100 kV. XPS measurements were obtained using a VG Scientific ESCALab 250 with a monochromatic Al Kα X-ray source (1486.6 eV). The spectra were calibrated in energy by setting the main C 1s component, assigned to aliphatic carbons, to 285 eV. The elementary analysis of the Bi and Te powders was carried out at the Institut des Sciences Analytiques, Service Central d'Analyse (SCA), in Villeurbanne (France).

Results

Characterization of the micro-hollow spheres

When decanethiol (DT) is introduced in the solution containing BiCl$_3$ and TeCl$_4$ in ethylene glycol (EG), two phases can be clearly distinguished in the flask: the polyol and the decanethiol are not miscible (usual DT/EG ratio: 1/11 vol.). The decanethiol phase turns to yellow very quickly. Upon heating from ambient temperature to 180 °C, the formation of the particles is evidenced by a modification of the solution color from light gray to dark gray or black. Under these conditions, XRD analysis confirms the formation of pure hexagonal Bi$_2$Te$_3$ (ICDD-JCPDS file 00-015-0863); (Fig. 1).

SEM-FEG micrographs from non-grinded samples reveal the formation of micro-hollow spheres (Fig. 2a, b). The diameter of the spheres is comprised between 8 and 15 μm. Upon closer examination, the internal surface of the sphere is more even compared to its external surface (see Figure S1 in Online Resource) which is made of hexagonal nanoplatelets giving a gypsum flower-like structure (Fig. 2c). The thickness of the hexagonal Bi$_2$Te$_3$ nanoplatelets composing the sphere wall ranges from 50 to 110 nm and diameters up to 1 μm. A TEM image of an isolated platelet and the corresponding diffraction pattern are displayed in Fig. 2d, e, respectively. They confirm the hexagonal structure of Bi$_2$Te$_3$ and show that the platelets are
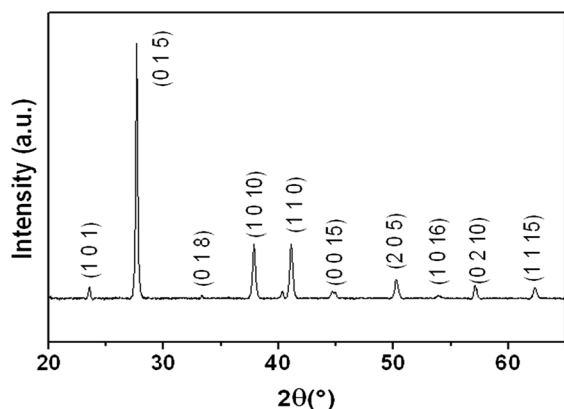
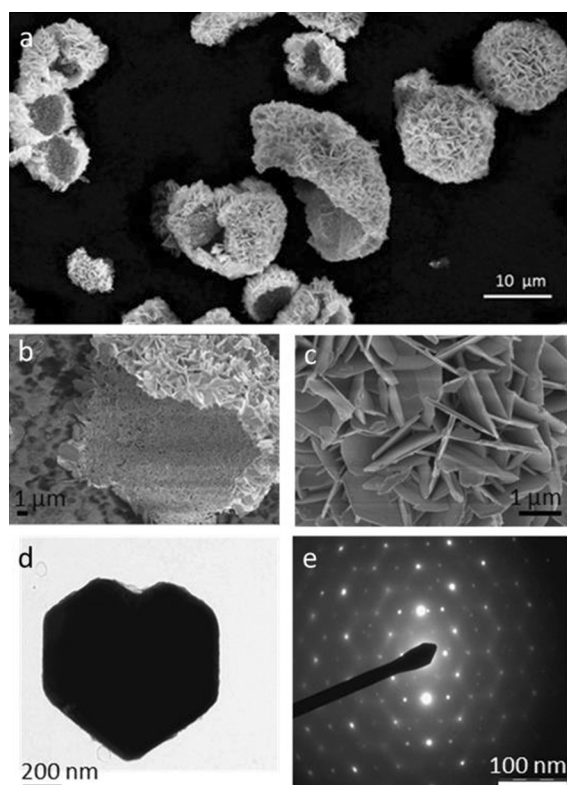**Fig. 1** XRD pattern of Bi_2Te_3 obtained in the DT/EG mixture

Fig. 2 a–c SEM-FEG micrographs of Bi_2Te_3 hollow spheres; **d** TEM micrograph of grinded Bi_2Te_3 powder and **e** the corresponding diffraction pattern

single crystals. The electron diffraction pattern was indexed within the R$\bar{3}$m crystal system taking the [001] zone axis. To our knowledge, no article has reported the formation of pure Bi_2Te_3-nanostructured hollow microspheres. Microspheres (~ 10 μm)

produced from the chemical transformation of BiOCl microspheres into Bi_2Te_3 were reported by Li et al. (2009) but were made of a mixture of Bi_2Te_3/BiOCl/$Bi_2Te_{3-x}O_x$. The synthesis of Bi_2Te_3 nanoplatelets of dimensions comparable to ours was also reported (Mehta et al. 2010; Son et al. 2012; Soni et al. 2012), as well as filled microspheres (~ 2 μm) made by ag-glomerated nanoplatelets (Wang et al. 2010).

After synthesis, neither infrared band characteristic of thiol nor significant weight loss in TGA analysis could be detected. The absence of a noticeable presence of decanethiol at the particle surface is also confirmed by elemental analysis results: less than 1 at.% of sulfur, 2–5 at.% of chlorine, and 3–8 at.% of carbon were detected using elemental analysis. XPS measurements revealed carbon, oxygen, bismuth, and tellurium core level peaks. The C 1s band was attributed to carbon contamination. The core level S 2p band could not be observed in such materials because of the strong intensity of the nearby bismuth 4f5/2 band; nevertheless, no signal characteristic of the S 2s band around 230 eV was detected either whereas this band could be easily detected when 1-decanethiol was grafted on the Bi_2Te_3 particles after the synthesis by chemical grafting (not shown here). Bi 4f and Te 3d high-resolution spectra are shown in Fig. 3.

The Bi 4f bands characteristics of Bi in Bi_2Te_3 are located at 157.7 and 163.0 eV for the Bi 4f7/2 and Bi 4f5/2, respectively. Bands characteristics of Te 3d5/2 and Te 3d3/2 in Bi_2Te_3 are observed at 572.3 and 582.6 eV, respectively. Particular care was taken to prevent oxidation of Bi_2Te_3 nanoparticles by keeping the powders under inert atmosphere and no band characteristic of oxidized Bi (usually observed at 158.5 eV for Bi_{ox} 4f7/2 and 163.8 eV for Bi_{ox} 4f5/2) or oxidized Te (usually observed at 575.7 eV for Te_{ox} 3d5/2 and 586.2 eV for Te_{ox} 3d3/2) in Bi_2Te_3 could be observed (Fu et al. 2012).

Mechanism of formation of the Bi_2Te_3 micro-hollow spheres: following the reactions steps

To gain further insights into the formation mechanism of hollow spheres, the solids obtained were charac-terized at different stages of the synthesis using XRD, SEM-FEG, EDX, X-ray fluorescence, and chemical analysis techniques. Analyses were performed on samples collected during the heating phase at 90, 120,

Fig. 3 Bi 4f (*top*) and Te 3d (*down*) XPS spectra obtained for Bi_2Te_3 samples
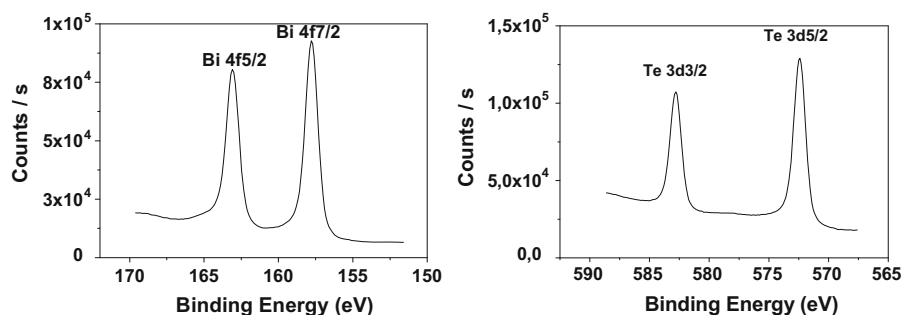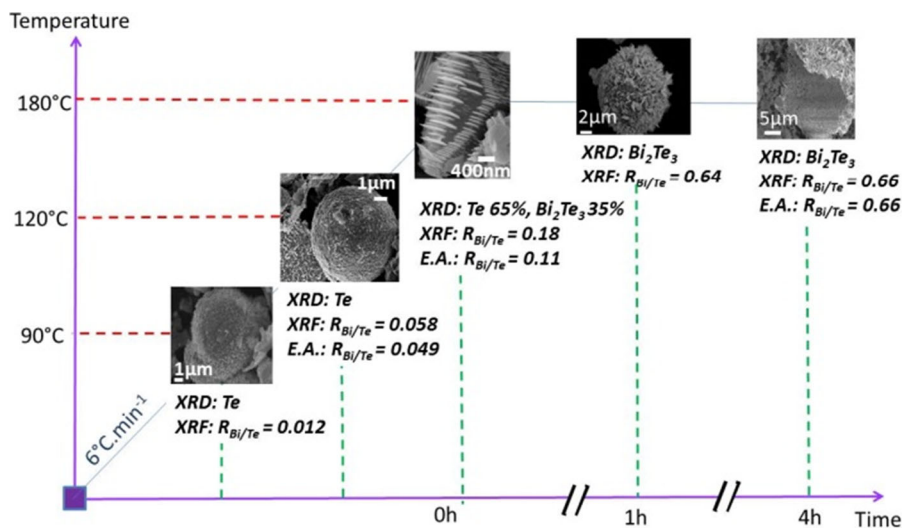

Fig. 4 Evolution of the sphere morphology by SEM, crystalline structure by XRD analysis, and chemical composition by X-ray fluorescence (XRF) and elemental analysis (EA); results as a function of temperature and time of reaction

and 180 °C and during the 180 °C stage after 1 and 4 h of reaction. The evolution of the solid morphology and the main characteristics are depicted in Fig. 4; XRD patterns and SEM images at different stages are given in Figure S2 and S3, respectively, in Online Resource. Spheres appear in the initial stage of the process. Nevertheless, at that point, according to XRD analysis, they are made of crystalline tellurium. During the heating process, at 90 and 120 °C, an increasing amount of Bi is detected along with Te according to both elemental analysis and X-ray fluorescence results; however, XRD measurements only confirm the presence of crystalline Te. Since the standard reduction potential of Te(IV)/Te(0) is higher (0.529 V) than that of Bi(III)/Bi(0) (0.308 V), Te is probably reduced at lower temperature. At 120 °C, a close examination of the sphere surface shows that the Te particles are slightly anisotropic and appear as short rods (see Figure S3(b) in Online Resource). From 120 °C, platelets progressively grow from the Te surface and

crystallize at the outer surface of the sphere. When the temperature reaches 180 °C, crystalline Bi_2Te_3 is detected along with crystalline Te using XRD and it is concomitant with the apparition of formed platelets at the surface of the spheres observed using SEM. After 1 h and more at 180 °C, according to XRD experiments, the spheres are made of pure crystalline Bi_2Te_3, and the Bi/Te ratio measured by X-ray fluorescence is in agreement with the existence of a single Bi_2Te_3 phase.

^{1}H NMR and GC–MS analyses of both the decanethiol and the ethylene glycol phases were also performed after different times of reaction to understand the role of the solvents/reducing agents. ^{1}H NMR spectra of pure decanethiol and the thiol-containing phase after the synthesis are depicted in Fig. 5.

After the reaction, using ^{1}H NMR, we found the half of the initial decanethiol (cf. experimental section for the attribution of peaks) according to Eq. 1, which
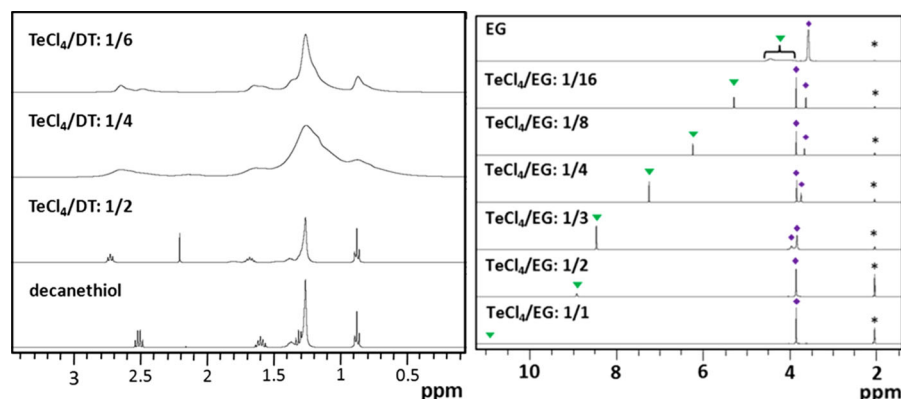
Fig. 5 ^{1}H NMR spectra of decanethiol (*top*) and of the decanethiol phase after reaction (*down*)

results in a 2/3 ratio of decanethiol to didecyldisulfide in the solution. This value corresponds to the quantity which is necessary to reduce both Te and Bi ions present in the solution to obtain Bi_2Te_3. The presence of didecyldisulfide was confirmed by GC–MS (Figure S4(a) in Online Resource). GC–MS also revealed that a large amount of the initial ethylene glycol was converted into diethylene glycol as well as a few oxidation products (Figure S4(b)).

(1)

Equation 1 Decanethiol-didecyldisulfide equilibrium.

It is well known that thiols are relatively unstable toward oxidation. Standard redox potential for the

half-Eq. 1 is relatively low (-1.0 to 0.5 V with respect to SCE, depending on the structure, solvent, and electrode material), and thiols are readily oxidized to corresponding disulfides by a variety of oxidizing agents (Witt et al. 2004). Reduction of disulfides into thiols is also straightforward and occurs in the presence of mild reducing agents. In our work, the redox mechanism is not a radical one since no other derivatives are observed. It is noteworthy that the oxidation of thiol into disulfide was not observed upon heating to 190 °C in ethylene glycol in the absence of metallic salts.

Mechanism of formation of the Bi_2Te_3 micro-hollow spheres: study of the salts in solution

Solution analysis was also carried out on each phase, decanethiol and ethylene glycol, using X-ray fluorescence and NMR techniques. First, when both precursors were introduced in the solution and before heating, the two phases of the solution were separated by decantation and analyzed by X-ray fluorescence. The spectra obtained for each phase are displayed in Fig. 6.

We observe with no ambiguity that the Bi ions are located in the polyol phase while Te ions can only be found in the decanethiol phase. Te preferentially dissolves in the thiol phase, and the yellow color cannot be attributed to $Bi(SR)_x$ complex formation as usually reported (Mai et al. 2011). Surprisingly, we have observed that, when $BiCl_3$ is added to a polyol-thiol solution, the thiol phase turns yellow immediately due to the Bi-thiol complex formation; nevertheless, there is a displacement of Bi ions from the thiol to the polyol phase upon $TeCl_4$ addition.

In order to deeper understand the state of the precursors in the two phases of the solution, the

Fig. 6 X-ray fluorescence spectra of the ethylene glycol phase (*top*) and the decanethiol phase (*down*) before heating

Fig. 7 ^{1}H NMR spectra of TeCl$_4$/DT (in CDCl$_3$) and TeCl$_4$/EG (in C$_2$D$_6$CO*). With *filled inverted triangle* the signal corresponding to free and bounded OH, and *filled diamond* the signal corresponding to –CH$_2$ of the EG molecules

precursors TeCl$_4$ and BiCl$_3$ were reacted independently in decanethiol and ethylene glycol.

How does TeCl$_4$ behave in DT and/or EG?

As mentioned previously, in the synthesis, medium tellurium ions migrate in the alcanethiol phase; nevertheless, EG molecules play a key role in the stability of Te-thiol complexes. Indeed, TeCl$_4$ precipitates immediately when it is in contact with decanethiol, while it stays stable for a few tens of minutes when it is first dissolved in EG and then the decanethiol is added. Using this 2-step procedure, Te(0) could be obtained from TeCl$_4$ (n_{thiol}/ n_{Te} = 50) with a yield of 90 %. SEM-FEG observations show the formation of aggregated polyhedral Te nanoparticles and Te nanorods (Figure S5 in Online Resource), similarly to those observed during the first stages of the synthesis performed in the presence of Bi precursors. TeCl$_4$/DT and TeCl$_4$/EG interactions were evidenced by ^{1}H NMR spectroscopy as shown in Fig. 7. Unlike Bi(SR)$_x$ complexes, Te(SR)$_x$ complexes could not be isolated since they are thermodynamically unstable toward decomposition to Te and the respective disulfide. As a result, from 1 to 4 equivalent of DT to TeCl$_4$, only didecyldisulfide can be found in the liquid phase analyzed by ^{1}H NMR spectroscopy in agreement with the stoichiometry of the oxido-reduction reaction between the Te^{4+} and the thiol. The reduction of Te^{4+} to Te(0) probably occurs through the formation of an intermediate complex such as Te(SR)$_2$ known to be thermally and photochemically unstable with respect to decomposition to elemental tellurium and disulfide (Fleischer et al. 2003).

For pure ethylene glycol in C$_2$D$_6$CO, the two signals characteristics of CH$_2$ and OH protons are located at 3.6 and between 4.6 and 3.7 ppm, respectively. As the ratio TeCl4/EG increases, the signal characteristic of OH protons (labeled ▼) is shifted from 4.6 to 10.9 ppm and its intensity decreases. The detailed interpretation of this shift, confirmed by NMR using HSQC sequence, is given in Figure S6 in Online Resource. At the same time, the main peak initially located at 3.87 ppm for TeCl$_4$/EG 1/1 splits and, while a part of the signal remains at the same shift, the outer signal (◆) shifts toward low ppm value. Both signals are attributed to protons from CH$_2$ in bounded and free ethylene glycol molecules. The ratio between OH and CH$_2$ signals fits well with the theoretical value calculated if only 1.5 molecules of EG is deprotonated to be covalently bounded to a Te center. Nevertheless, above 1.5 EG per TeCl$_4$, even if EG molecules are not covalently bounded to Te^{4+} centers, they are affected by the presence of Te ions in the solution perhaps to form a larger structure involving several EG molecules. To conclude, it seems that a mixed complex with thio- and oxo-ligands is responsible for the particular stability of TeCl$_4$ under these conditions.

How does BiCl$_3$ behave in DT and/or EG?

The reduction of BiCl$_3$ in polyol in the presence of DT yields to rhombohedric Bi particles (Figure S7 in Online Resource) whereas bismuth oxychloride (ICDD-JCPDS file 00-006-0249) was obtained along with rhombohedric Bi when no thiol was added in the polyol medium. Thiol molecules are reducing agents
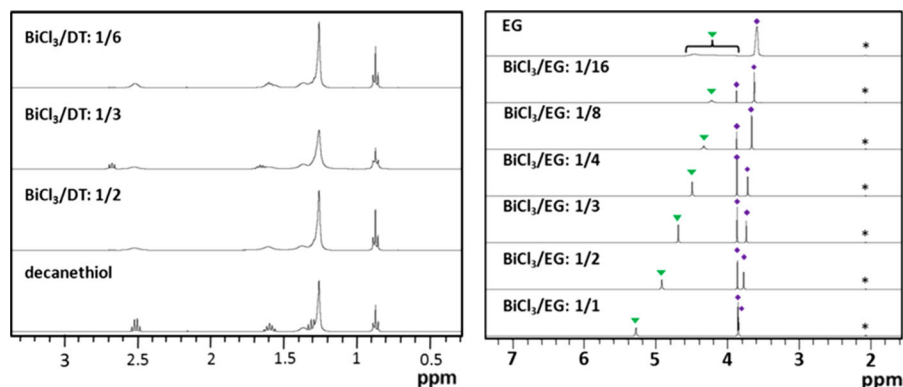
Fig. 8 ^{1}H NMR spectra of BiCl$_3$/DT (in CDCl$_3$) and BiCl$_3$/EG (in C$_2$D$_6$CO *) solutions prepared at rT. *Filled inverted triangle* signal corresponding to free and bounded OH, and *filled diamond* signal corresponding to –CH$_2$ of the EG molecules

and favor Bi formation; moreover, they have a tendency to form stable complexes with Bi^{3+} ions thus preventing the formation of bismuth oxychloride (Mai et al. 2011). ^{1}H NMR spectra of BiCl$_3$ with 1–6 equivalents of DT shown in Fig. 8 confirm the Bi(SR)$_3$ complex formation at room temperature. Indeed, the triplet attributed to H$_k$ (Eq. 1) and located at 1.31 ppm disappears upon addition of BiCl$_3$ into the DT solution whereas peaks characteristics of H$_a$ and H$_b$ are broadened due to rapid exchange of thiol ligands. At room temperature, the Bi-thiol complex remains stable for the most part, and, after 1 week, only a slight amount of oxidized alcanethiol into didecyldisulfide is detected along with DT.

As observed for TeCl$_4$/EG, as the BiCl$_3$/EG ratio decreases from 1/1 to 1/16, the signal characteristic of OH protons (labeled ▼) and the signal attributed to protons from CH$_2$ in bounded EG molecules (◆) shift toward low ppm values (^{1}H NMR spectra shown in Fig. 8). This confirms that ethylene glycol forms a complex with Bi^{3+} ions. Nevertheless, for BiCl$_3$, the relative integration of OH and CH$_2$ signals implies that EG molecules interacting with Bi^{3+} centers are not deprotonated and only one of the two hydroxyl group interacts up to 4 EG molecules per Bi. Above this value, free EG molecules coexist with Bi–EG complexes.

Discussion

The above-mentioned results allowed us to propose a mechanism which is illustrated in Fig. 9.

The addition of decanethiol to a solution of Bi and Te salts dissolved in ethylene glycol causes the migration of Te ions into the decanethiol droplets whereas the Bi ions remains in the continuous EG phase. This results in a biphasic medium in which the two different precursors are dissolved in two different solvents as illustrated in step 1 of Fig. 9. The preferential solubility of Te and Bi ionic species in DT and EG, respectively, can be rationalized by the Pearson theory. It is commonly admitted that O^{2-} and OH$^-$ are both very hard bases while S^{2-} and RS$^-$ are rather soft. For elements of variable valence, there is usually a smooth in hardness as the oxidation state increases since the radius decreases and the electron density increases. The difference in hardness between Bi^{3+} and Te^{4+} is not as clearly pronounced as for O and S; nevertheless, according to Pearson work (Pearson 1968), Te^{4+} belongs to soft acids while Bi^{3+} is more borderline. From these considerations, it seems that Bi^{3+} would preferentially dissolve in ethylene glycol (hard–hard), while Te^{4+} would preferentially dissolve in the thiol phase (soft–soft). In addition, if we consider that Te^{4+} is, at least to some extent, reduced into Te^{2+} (even softer that Te^{4+} because of its lower oxidation state), Te ionic species would be located in the thiol phase. This theory is in agreement with what has been experimentally observed in this work and could potentially guide further experiments for two-phase reactions.

In a second step (step 2, Fig. 9), the spherical liquid–liquid interface between the two phases obtained here is the favored location for the reduction of Te^{4+} into Te(0) and further agglomeration of Te nanoparticles since polar groups (–SH and/or –OH) solvating particles seeds are preferentially located toward the highly polar continuous medium. Closer
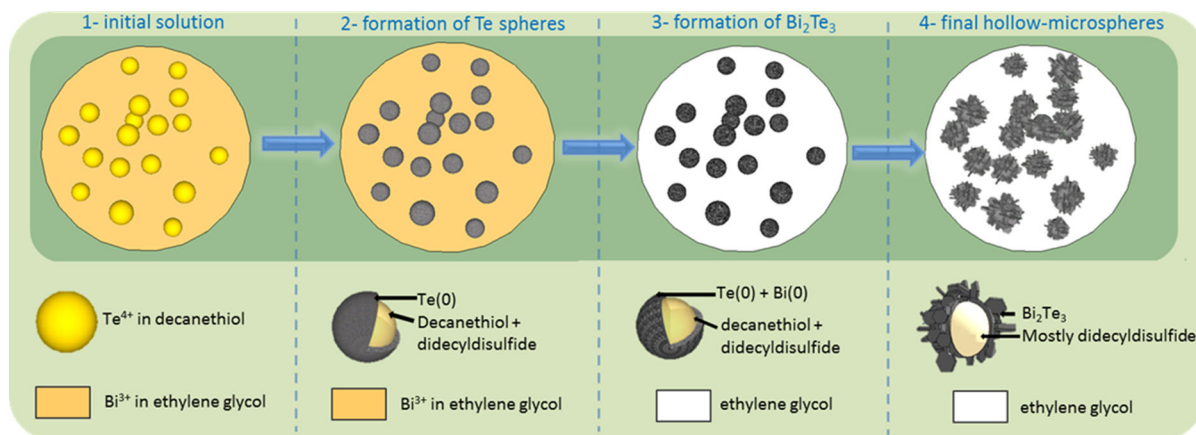
Fig. 9 Illustration of mechanism of formation of Bi_2Te_3 nanostructured hollow microspheres

examination of the sphere surface at the first stages of the reaction shows that the Te particles are slightly anisotropic and appear as short rods. Subsequently, there is a growth of Bi_2Te_3 nanoplatelets that lead to the final gypsum flower-like structure. The growth of Bi_2Te_3 platelets perpendicularly to the *c*-axis of Te rods has already been reported (Mai et al. 2011; Zhang et al. 2012a) and can account for the particular morphology obtained. Regarding the progressive transformation of Te into Bi_2Te_3, two mechanisms have been proposed: either Te(0) is further reduced into Te^{2-} and react with Bi^{3+}, or the formation of Bi_2Te_3 results from a dissolution-precipitation process of Te(0) and Bi(0) (Zhang et al. 2012b; Zhou et al. 2006). Considering the potentials $E°(Te^{4+}/Te) = 0.529$ V, $E°(Bi^{3+}/Bi) = 0.308$ V, and $E°(Te/Te^{2-}) = -1.14$ V (Zhou et al. 2006), the latest mechanism is more probable since, after Te^{4+} reduction, Bi^{3+} reduction will be favored and the sphere structure is preserved. After Bi(0) atoms deposition onto Te(0) nanorods, Bi_2Te_3 nanoplatelets grow at the outer surface of the sphere (step 3, Fig. 9) and consolidate the sphere structure.

The formation of elemental Te and subsequent reduction of Bi^{3+} to form Bi_2Te_3 nanoparticles during synthesis performed in the presence of alcanethiol has already been reported (Wang et al. 2006). However, decanethiol was presented as a capping ligand during the synthesis of Te or Bi_2Te_3 nanoparticles. In the present work, the thiol molecules were clearly identified both as a complexing and reducing agent. The role of decanethiol in the reduction of the inorganic

salts was clearly evidenced by ^{1}H NMR studies performed on the thiol phase at different stages of the reaction: decanethiol is oxidized into disulfide and its final concentration corresponds to what is expected for the reduction of both Bi and Te ions. Indeed, since the initial thiol/Te ratio is 16.5, the amount of thiol that should be converted into disulfide should be 24 % if it was solely participating in Te^{4+} ions reduction. If we consider that the decanethiol also participate in Bi^{3+} ions reduction, 36 % of the initial thiol contained in the solution should be converted into disulfide. Experimentally, when the reaction is performed without $BiCl_3$ (only $TeCl_4$), the amount of thiol converted into disulfide is of 30 % whereas when the synthesis is performed with both precursors, 50 % of the initial thiol is converted into disulfide. Even if the amount of thiol converted into disulfide is slightly larger than the expected value, these results show that the decanethiol also contributes to the reduction of Bi^{3+} ions. XRD analyses of the solid materials obtained with different DT/precursor ratio corroborate this fact as illustrated in Fig. 10.

When the $DT/TeCl_4$ ratio in the synthesis medium is lower than 16.5, elemental Te is detected along with Bi_2Te_3. As the $DT/TeCl_4$ ratio increases, the Bi_2Te_3 to Te ratio increases. Both phases were also observed on SEM-FEG images where the hexagonal Bi_2Te_3 platelets already organized into microspheres coexist with tellurium. Above a $DT/TeCl_4$ ratio equal to 16.5, pure Bi_2Te_3 is obtained after only 60 min of reaction. All the results confirm that the decanethiol first reduces Te^{4+} which has a higher potential ($E°(Te^{4+}/Te) = 0.529$ V)

Fig. 10 X-ray diffractograms of the powders obtained for different decanethiol/TeCl$_4$ ratios in a typical synthesis (BiCl$_3$, TeCl$_4$, DT and EG). Percentages of the different phases were calculated using Rietveld's software MAUD
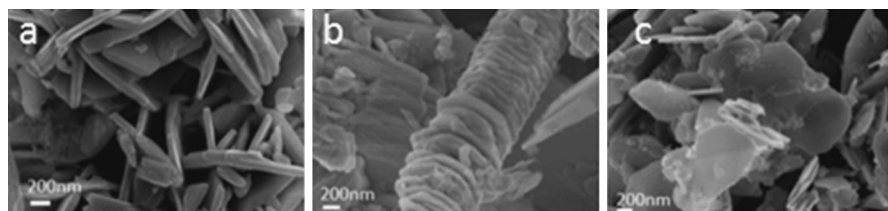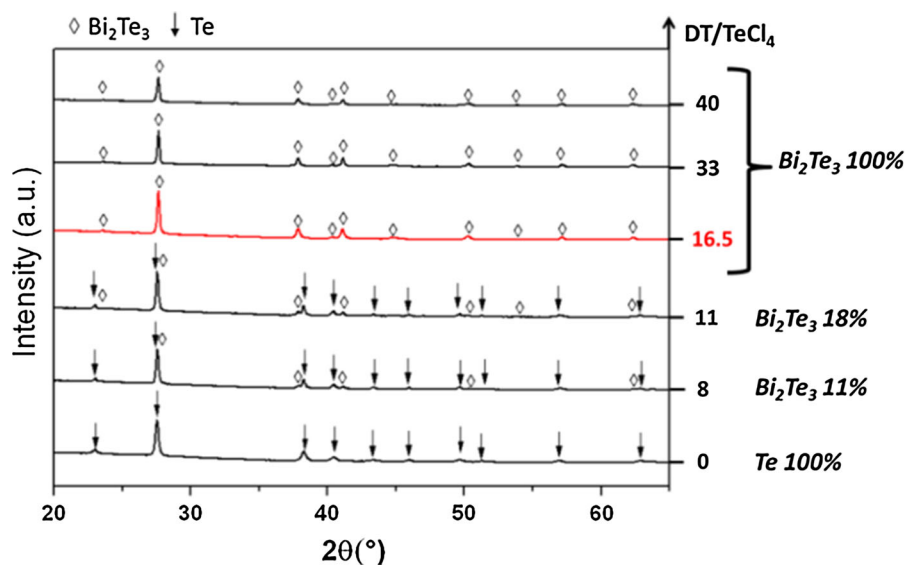

Fig. 11 Influence of stirring conditions on Bi$_2$Te$_3$ morphology with **a** magnetic stirring **b** no stirring **c** sonication of the solution during the synthesis

than Bi^{3+}. Unlike in other reported work (Mehta et al. 2010), using this procedure, the microsphere formation does not result from the aggregation of nanoplates but from the growth of Bi$_2$Te$_3$ nanoplates at the surface of Te spheres by progressive Bi reaction. SEM images clearly show the formation of Te spheres at the initial stage of the reaction and their progressive transformation into nanostructured micro-hollow spheres. These results suggest that Bi$_2$Te$_3$ nanoplatelets progressively grow at the thiol/polyol interface. The growth orientation is favored at the external surface of the sphere since the ethylene glycol continuous phase acts as the main reservoir for Bi ions.

As for any emulsion, the formation of droplets is dictated by the experimental conditions and in particular by the stirring of the solution as illustrated in Fig. 11. It is to note that, according to XRD measurements, pure Bi$_2$Te$_3$ is obtained in all cases.

Upon stirring, the formation of an emulsion leads to the formation of Te(0) spheres and the subsequent nanoplatelets growth toward the external sphere surface (Fig. 11a). When the solution is not stirred, the two

phases are well separated with the DT at the top since its density is lower than that of the polyol. The reaction still occurs at the solvents interface and lead to a particular columnar morphology as it can be observed in Fig. 11b. The columnar morphology results from an oriented growth of Bi$_2$Te$_3$ nanoplatelets perpendicularly to the main growth axis of initially formed Te nanorods. The length of the columns either results from long Te rods that can form in situ since there are not constraints by a limited growth space as in the case of emulsion synthesis, or from an oriented attachment of small Bi$_2$Te$_3$ columns formed on shorter Te rods. When sonication is applied during the synthesis, droplets are constantly broken and no spheres can be observed (Fig. 11c). The formation of the emulsion is a key parameter in micro-hollow sphere synthesis.

Conclusions

We have developed a simple approach to obtain Bi$_2$Te$_3$ micro-hollow spheres composed of

monocrystalline Bi_2Te_3 nanoplatelets. We have proven ^{1}H NMR to be a powerful tool for deeper understanding the nanoparticles formation and elucidate the reducing mechanisms occurring in complex solvent systems. This also opens new doors for the exploration of nanoparticles formation mechanisms which is of particular interest to provide a better control and eventually predict particles morphology. The emulsion technique based on the differential solubility of precursor salts in two different reducing solvents could potentially open new ways for the preparation of solid solution hollow sphere, in particular, in microfluidic systems which allow a perfect control of droplet size. Reactant concentrations, surfactant/precursor ratio, and type of precursors have to be adjusted to obtain such systems. Using different precursor salts and playing on the reducing strength of both solvents give opportunities for the synthesis of new hierarchically structured alloys. As mentioned in the introductive part of the paper, these particular hierarchical hollow-structured materials are of great interest in particular for applications in energy-related fields. Indeed, next step is to disperse the obtained nanostructured spheres in a conducting organic polymer in order to prepare hybrid films for flexible and easily processable thermoelectric devices.

References

Brayner R, Fievet F, Coradin T (2013) Chapter 1: the polyol process. Nanomaterials: a danger or a promise. Springer, New York, pp 1–25

Fievet F (2000) Metals. Polyol Process Surfactant Sci Ser 92:460–496

Fievet F, Lagier JP, Blin B, Beaudoin B, Figlarz M (1989) Homogeneous and heterogeneous nucleations in the polyol process for the preparation of micron and submicron size metal particles. Solid State Ionics 32–33:198–205. doi:10.1016/0167-2738(89)90222-1

Fleischer H, Mitzel NW, Schollmeyer D (2003) Tellurium(II) dialkanethiolates: np(S)-σ*(Te-S') orbital interactions determine the 125Te NMR chemical shift, and the molecular and crystal structure. Eur J Inorg Chem 2003:815–821. doi:10.1002/ejic.200390111

Fu J, Song S, Zhang X, Cao F, Zhou L, Li X, Zhang H (2012) Bi2Te3 nanoplates and nanoflowers: synthesized by hydrothermal process and their enhanced thermoelectric properties. CrystEngComm 14:2159–2165. doi:10.1039/c2ce06348d

Gao J, Zhang B, Zhang X, Xu B (2006) Magnetic-dipolar-interaction-induced self-assembly affords wires of hollow nanocrystals of cobalt selenide. Angew Chem Int Ed 45:1220–1223. doi:10.1002/anie.200503486

Guo L et al (2007) Uniform magnetic chains of hollow cobalt mesospheres from one-pot synthesis and their assembly in solution. Adv Funct Mater 17:425–430. doi:10.1002/adfm.200600415

Hu J, Chen M, Fang X, Wu L (2011) Fabrication and application of inorganic hollow spheres. Chem Soc Rev 40:5472–5491. doi:10.1039/c1cs15103g

Jiang Y, Zhu Y-J, Chen L-D (2007) Microwave-assisted preparation of Bi2Te3 hollow nanospheres. Chem Lett 36:382–383. doi:10.1246/cl.2007.382

Kanatzidis MG (2010) Nanostructured thermoelectrics. The new paradigm? Chem Mater 22:648–659. doi:10.1021/cm902195j

Kim KT, Kim D-W, Ha GH (2010a) Direct synthesis of Te/Bi2Te3 nanocomposite powders by a polyol process. Res Chem Intermed 36:835–841. doi:10.1007/s11164-010-0188-4

Kim KT, Lee HM, Kim DW, Kim KJ, Ha GH, Lee G-G (2010b) Bismuth-telluride thermoelectric nanoparticles synthesized by using a polyol process. J Korean Phys Soc 57:1037–1040. doi:10.3938/jkps.57.1037

Kim C, Kim DH, Han YS, Chung JS, Park S, Kim H (2011) Fabrication of bismuth telluride nanoparticles using a chemical synthetic process and their thermoelectric evaluations. Powder Technol 214:463–468. doi:10.1016/j.powtec.2011.08.049

Lai X, Halpert JE, Wang D (2012) Recent advances in micro-/nano-structured hollow spheres for energy applications: from simple to complex systems energy. Environ Sci 5:5604–5618. doi:10.1039/c1ee02426d

Li Y, Shi J, Hua Z, Chen H, Ruan M, Yan D (2003) Hollow spheres of mesoporous aluminosilicate with a three-dimensional pore network and extraordinarily high hydrothermal stability. Nano Lett 3:609–612. doi:10.1021/nl034134x

Li L, Cao R, Wang Z, Li J, Qi L (2009) Template synthesis of hierarchical Bi2E3 (E = S, Se, Te) core-shell microspheres and their electrochemical and photoresponsive properties. J Phys Chem C 113:18075–18081. doi:10.1021/jp906407n

Liu H, Qu J, Chen Y, Li J, Ye F, Lee JY, Yang J (2012) Hollow and cage-bell structured nanomaterials of noble metals. J Am Chem Soc 134:11602–11610. doi:10.1021/ja302518n

Lu Y, McLellan J, Xia Y (2004) Synthesis and crystallization of hybrid spherical colloids composed of polystyrene cores and silica shells. Langmuir 20:3464–3470. doi:10.1021/la036245h

Mai NT, Mott D, Nguyen TBT, Osaka I, Maenosono S (2011) Study on formation mechanism and ligand-directed architectural control of nanoparticles composed of Bi, Sb and Te: towards one-pot synthesis of ternary (Bi,Sb)2Te3 nanobuilding blocks. RSC Adv 1:1089–1098. doi:10.1039/c1ra00069a

Mehta RJ, Karthik C, Singh B, Teki R, Borca-Tasciuc T, Ramanath G (2010) Seebeck tuning in chalcogenide

nanoplate assemblies by nanoscale heterostructuring. ACS Nano 4:5055–5060. doi:10.1021/nn101322p

Mott D, Mai NT, Thuy NTB, Maeda Y, Linh TPT, Koyano M, Maenosono S (2011) Bismuth, antimony and tellurium alloy nanoparticles with controllable shape and composition for efficient thermoelectric devices. Phys Status Solidi A 208:52–58. doi:10.1002/pssa.201026485

Nakashima T, Kimizuka N (2003) Interfacial synthesis of hollow TiO_2 microspheres in ionic liquids. J Am Chem Soc 125:6386–6387. doi:10.1021/ja034954b

Pearson RG (1968) Hard and soft acids and bases (HSAB), part I: fundamental principles. J Chem Educ 45:581–587. doi:10.1021/ed045p581

Purkayastha A, Lupo F, Kim S, Borca-Tasciuc T, Ramanath G (2006) Low-temperature, template-free synthesis of single-crystal bismuth telluride nanorods. Adv Mater 18:496–500. doi:10.1002/adma.200501339

Son JS et al (2012) n-Type nanostructured thermoelectric materials prepared from chemically synthesized ultrathin Bi_2Te_3 nanoplates. Nano Lett 12:640–647. doi:10.1021/nl203389x

Soni A, Yanyuan Z, Ligen Y, Aik MKK, Dresselhaus MS, Xiong Q (2012) Enhanced thermoelectric properties of solution grown Bi_2Te_3-xSex nanoplatelet composites. Nano Lett 12:1203–1209. doi:10.1021/nl2034859

Sun Y, Mayers B, Xia Y (2003) Metal nanostructures with hollow interiors. Adv Mater 15:641–646. doi:10.1002/adma.200301639

Wang Y, Su F, Lee JY, Zhao XS (2006) Crystalline carbon hollow spheres, crystalline carbon-SnO_2 hollow spheres, and crystalline SnO_2 hollow spheres: synthesis and performance in reversible Li-ion storage. Chem Mater 18:1347–1353. doi:10.1021/cm052219o

Wang T et al (2010) Microsphere bouquets of bismuth telluride nanoplates: room-temperature synthesis and thermoelectric properties. J Phys Chem C 114:1796–1799. doi:10.1021/jp908727b

Witt D, Klajn R, Barski P, Grzybowski BA (2004) Applications, properties and synthesis of ω-functionalized n-alkanethiols and disulfides—the building blocks of self-assembled monolayers. Curr Org Chem 8:1763–1797. doi:10.2174/1385272043369421

Yang HG, Zeng HC (2004) Self-construction of hollow SnO2 octahedra based on two-dimensional aggregation of nanocrystallites. Angew Chem Int Ed 43:5930–5933. doi:10.1002/anie.200461129

Zhang G, Fang H, Yang H, Jauregui LA, Chen YP, Wu Y (2012a) Design principle of telluride-based nanowire heterostructures for potential thermoelectric applications. Nano Lett 12:3627–3633. doi:10.1021/nl301327d

Zhang G, Kirk B, Jauregui LA, Yang H, Xu X, Chen YP, Wu Y (2012b) Rational synthesis of ultrathin n-type Bi_2Te_3 nanowires with enhanced thermoelectric properties. Nano Lett 12:56–60. doi:10.1021/nl202935k

Zhao C-X, Middelberg APJ (2013) One-step fabrication of titania hollow spheres by controlled interfacial reaction in a droplet-based microfluidic system. Microfluid Nanofluid 14:703–709. doi:10.1007/s10404-012-1088-2

Zhou B, Zhao Y, Pu L, Zhu J-J (2006) Microwave-assisted synthesis of nanocrystalline Bi_2Te_3. Mater Chem Phys 96:192–196. doi:10.1016/j.matchemphys.2005.07.010

Zhu H, Wang J, Xu G (2009) Fast synthesis of Cu_2O hollow microspheres and their application in DNA biosensor of hepatitis B virus. Cryst Growth Des 9:633–638. doi:10.1021/cg801006g